HHS Public Access

Author manuscript

Ophthalmology. Author manuscript; available in PMC 2016 January 04.

Published in final edited form as:

Ophthalmology. 2015 September ; 122(9): 1786–1794. doi:10.1016/j.ophtha.2015.06.001.

Bruch's Membrane Opening-Minimum Rim Width and Retinal Nerve Fibre Layer Thickness in a Normal White Population. A Multi-centre Study

Balwantray C. Chauhan[1], **Vishva M. Danthurebandara**[1], **Glen P. Sharpe**[1], **Shaban Demirel**[2], **Christopher A. Girkin**[3], **Christian Y. Mardin**[4], **Alexander F. Scheuerle**[5], and **Claude F. Burgoyne**[2]

[1]Department of Ophthalmology and Visual Sciences, Dalhousie University, Halifax, NS, Canada

[2]Devers Eye Institute, Portland, OR

[3]Department of Ophthalmology, University of Alabama at Birmingham, AL

[4]Department of Ophthalmology, University of Erlangen, Erlangen, Germany

[5]Department of Ophthalmology, University of Heidelberg, Germany

Abstract

Objective—Conventional optic disc margin-based neuroretinal rim measurements lack a solid anatomical and geometrical basis. An optical coherence tomography (OCT) index, Bruch's membrane opening minimum rim width (BMO-MRW), addresses these deficiencies and has higher diagnostic accuracy for glaucoma. We characterized BMO-MRW and peripapillary retinal nerve fiber layer thickness (RNFLT) in a normal population.

Design—Multi-centred cross-sectional study.

Participants—Normal White subjects.

Methods—Approximately equal number of subjects in each decade group (20–90 years) was enrolled in 5 centers. Subjects had normal ocular and visual field examinations. We obtained OCT images of the optic nerve head (24 radial scans) and peripapillary retina (1 circular scan). The angle between the fovea and BMO center (FoBMO), relative to the horizontal axis of the image frame, was first determined and all scans were acquired and analyzed relative to this eye-specific FoBMO axis. Variation of BMO-MRW and RNFLT was analyzed with respect to age, sector and BMO shape.

Main Outcome Measures—Age-related decline and between-subject variability in BMO-MRW and RNFLT.

Address for correspondence: Balwantray C Chauhan, Department of Ophthalmology and Visual Sciences, Dalhousie University, 1276 South Park Street, 2W Victoria, Halifax, Nova Scotia, Canada B3H 2Y9. Tel: 902-473-3202 Fax: 902-473-2839 bal@dal.ca.

Financial/conflict of interest disclosure: B.C. Chauhan, Heidelberg Engineering (S). S. Demirel, Heidelberg Engineering (S), C.A. Girkin, Heidelberg Engineering (S), A.F. Scheuerle, Heidelberg Engineering (S), C.Y. Mardin, Heidelberg Engineering (S), C.F. Burgoyne, Heidelberg Engineering (S).

Results—There were 246 eyes of 246 subjects with a median age of 52.9 (range, 19.8 to 87.3) years. The median FoBMO angle was −6.7° (range, 2.5° to −17.5°). BMO was predominantly vertically oval with a median area of 1.74 mm^2 (range, 1.05 to 3.40 mm^2). Neither FoBMO angle nor BMO area was associated with age or axial length. Both global mean BMO-MRW and RNFLT declined with age at a rate of −1.34 μm/y and −0.21 μm/y, equivalent to 4.0% and 2.1% loss per decade of life, respectively. Sectorally, the most rapid decrease occurred inferiorly and the least temporally, however, the age association was always stronger with BMO-MRW than with RNFLT. There was a modest relationship between mean global BMO-MRW and RNFLT (r = 0.35), while sectorally the relationship ranged from moderate (r = 0.45, inferotemporal) to non-existent (r = 0.01, temporal).

Conclusions—There was significant age-related loss of BMO-MRW in healthy subjects and notable differences between BMO-MRW and RNFLT in their relationship with age and between each other. Adjusting BMO-MRW and RNFLT for age and sector is important in ensuring optimal diagnostics for glaucoma.

Spectral domain optical coherence tomography (OCT) has become an important imaging modality in the diagnosis and follow-up of glaucoma and retinal diseases. Furthermore, OCT has permitted important anatomical insights into the optic nerve head (ONH) structures that correspond to the clinically perceived optic disc margin[1, 2] and visualization of deep ONH structures such as the anterior laminar surface[3, 4] and the termination of the Bruch's membrane/retinal pigment epithelium complex within the ONH.[3, 4, 2]

Optic disc margin-based indices that quantify the neuroretinal rim, such as cup-disc ratio and rim area lack a solid anatomical and geometrical rationale. [5, 2] Conventional fundoscopy and disc photography do not permit clinicians to visualize critical anatomy that delineates the outer edge of the rim, principally because of extensions of Bruch's membrane well inside the clinical disc margin, that are present in variable amounts in all eyes,[2] and that yield critical errors in rim estimates.[5]

Recently, we and others[6–8, 5] have proposed an anatomically and geometrically accurate neuroretinal rim parameter which is one aspect of an OCT-based paradigm change in the clinical assessment of the ONH.[9] This parameter, Bruch's membrane opening minimum rim width (BMO-MRW)[5] measures the rim from a logical outer border of the neuroretinal rim, that is BMO, which represents the maximum aperture at the level of the ONH through which retinal ganglion cell axons can pass. It is also a geometrically accurate measurement as it measures the minimum rim width from BMO to the internal limiting membrane, and not conventionally along or parallel to the fixed plane of the disc margin or BMO. Recent publications from our groups and others have shown a higher diagnostic accuracy for glaucoma with BMO-MRW[10–12] and a stronger relationship with the visual field compared to conventional rim parameters. [13, 12, 14]

The orientation of the fovea relative to BMO impacts the accuracy of sector-based rim measurements of the ONH, and the peripapillary and macular retinal nerve fiber layer thickness (RNFLT).[9] While the mean fovea-BMO center (FoBMO) angle is around −7°, relative to the horizontal axis of the image frame, it can vary from 6° to −17° among individuals.[15] As a result, the current strategy of assigning sectors relative to the fixed

horizontal and vertical axes of the imaging device could result in artificially large variability among individuals (Fig. 1) and decrease diagnostic accuracy. It also results in significant differences in BMO-MRW in the majority of clock hour sectors compared to computation according to the FoBMO axis.[15] For these reasons, we recently proposed that both image acquisition and analysis be performed according to the individual subject's FoBMO axis.[9]

Incorporating BMO-MRW into clinical devices requires a robust description of BMO-MRW and the parameters that could influence it, including age and BMO area, in order to phenotype the normal ONH and construct prediction intervals to determine the likelihood that a test result is within normal limits. The objective of this research was to provide such a description of BMO-MRW in data acquired and analyzed according to the eye-specific FoBMO axis in a multicenter study with a White population.

METHODS

Participants

Study participants of self-identified Caucasian descent were recruited in 5 centres; one in Canada, two in the United States and two in Germany. The study was approved by the Ethics Review Board at each of the institutions. In accordance with the declaration of Helsinki, all subjects gave informed consent to participate.

A verbal screening for participation was first conducted. A medical history was then obtained, followed by an ocular health assessment that included visual acuity measurement with a standard Snellen or Early Treatment Diabetic Retinopathy Study (ETDRS) chart, refraction, keratometry and axial length measurement. Visual field examination was then conducted with standard automated perimetry (Humphrey Field Analyzer (Carl Zeiss Meditec, Dublin, CA), with the 24–2 Swedish Interactive Thresholding Algorithm), repeated once if not deemed reliable or within normal limits (see below), OCT examination (see below), ophthalmoscopic examination of the posterior pole and ONH stereophotography. Finally, Goldmann tonometry and pachymetry were performed.

Subjects were included into the study if all the following inclusion criteria were met: (1) age between 18 and 90 years; (2) clinically normal eye examination without clinically significant vitreo-retinal or choroidal disease and prior intraocular surgery except cataract or refractive surgery; (3) intraocular pressure ≤ 21 mm Hg; (4) best corrected visual acuity ≥ 20/40; (5) refractive error within 6 D spherical error and 2 D astigmatic error; and (6) normal visual field with the Glaucoma Hemifield Test and Mean Deviation within normal limits. Subjects were excluded if any of the following were found: (1) unreliable visual field examination based on the reliability indices and the perimetrist's notes; (2) ONH photographs of insufficient quality; (3) OCT images of insufficient quality (see below).

All test procedures were carried out in both eyes of each subject, if eligible, however, for the purpose of this study, data analysis was performed in one randomly selected eye only.

Spectral domain optical coherence tomography

The ONH, peripapillary RNFL and macula were imaged with OCT (Spectralis, Heidelberg Engineering GmbH, Heidelberg, Germany) with prototype software (Heyex VV, Heidelberg Engineering).

A scan pattern containing 24 radially equidistant B-scans, each subtending 15° was first centred on the ONH. The foveal pit was manually identified with a live B-scan, followed by the 2 BMO points in each of two radial B-scans that were perpendicular to each other. These points were used to identify the FoBMO axis which served as a reference for the scans. Radial B-scans, each containing 1,536 A-scans and which represented the average of 25 individual scans were obtained in standard and enhanced depth imaging modes. Circular peripapillary scans with 768 A-scans each which represented the average of 100 individual scans were obtained with circles subtending 12°, 14° and 16° and also diameters measuring 3.5 mm, 4.1 mm and 4.7 mm to measure RNFLT. Finally, also with reference to the FoBMO axis, horizontal (61 B-scans subtending 30° × 25°) and vertical (19 B-scans subtending 15° × 30°) volume scans centred on the fovea were obtained. Axial length and corneal curvature measurements were entered into the instrument software to ensure accurate scaling of all measurements.

Eyes with poor quality OCT scans (truncated B-scans where the internal limiting membrane could not be segmented and/or image quality score < 20) were excluded.

For brevity, in this report, only results with the standard ONH and the 3.5 mm diameter RNFL scans were analyzed and presented.

Data analysis

All eyes were converted to right eye format. The software automatically segmented the internal limiting membrane and the 48 BMO points from the 24 radial B-scans. The segmentations was manually checked in each B-scan and corrected when necessary. The BMO-based parameters were computed as described before.[5] Briefly, the shortest distance from each BMO point to the internal limiting membrane in each B-scan was defined as BMO-MRW (48 values per eye). The BMO points were fitted with a spline to derive a closed curve to represent the BMO around the ONH. The torsion angle of the ONH was defined as the orientation of the long axis of BMO (the radial with the longest length) relative to the perpendicular of the FoBMO axis (Fig. 2, available at http://aaojournal.org). The global and the four 40° (superonasal, inferonasal, inferotemporal and superotemporal), one 90° (temporal) and one 110° (nasal) sectoral BMO-MRW values were computed. The corresponding global and sectoral peripapillary RNFLT values were also computed. Data were also analysed for the twelve 30° clock-hour sectors. For each subject, all orientations were relative to the FoBMO axis.

Strengths of associations between variables were determined with Pearson's correlation coefficient. Rank order correlations were determined with Spearman's correlation coefficient. The annual rates of BMO-MRW and RNFLT loss were adjusted for significant covariates. The measured BMO-MRW and RNFLT values were linearly extrapolated at

each degree around BMO and the RNFLT scan circle, respectively. Thereafter, the prediction limits for BMO-MRW and RNFLT were derived.

RESULTS

There were 259 subjects enrolled and tested of whom 13 (5.0%) were excluded because of poor OCT image quality. Among the remaining 246 subjects, there were approximately 35–40 subjects in each decade group, except the 80–89 year old group, which contained 14 subjects. The median (range) age was 52.9 (19.8 to 87.3) years.

The FoBMO angle varied widely (Fig. 3), with a median of −6.7° (range, 2.5° to −17.5°), relative to the horizontal axis of the image frame. The FoBMO angle was unrelated to age (r = −0.11, P = 0.09) or axial length (r = 0.11, P = 0.08). The median BMO area was 1.74 mm^2 (range, 1.05 to 3.40 mm^2, Fig. 4, available at http://aaojournal.org) and was similarly unrelated to age (r = −0.10, P = 0.14) or axial length (r = −0.02, P = 0.81).

Torsion angle was not correlated to the FoBMO angle (r = 0.12, P = 0.06). BMO was predominantly vertically oval in shape with the BMO long axis situated within the 12 ‘o’ clock 30° sector in 116 (47%) subjects. The median torsion angle was −15° (range, −83° to 90°, Fig. 3).

Both global mean BMO-MRW and RNFLT were significantly associated with age (P < 0.01, Fig. 5). Global mean BMO-MRW loss (adjusted for BMO area and BMO long axis length) was −1.34 μm/y (R^2 = 0.25, P < 0.01) while RNFLT loss (adjusted for BMO area, BMO long axis length and axial length) was −0.21 μm/y (R^2 = 0.24, P < 0.01). Relative to median values, these rates are equivalent to 4.0% and 2.1% loss per decade of life in global mean BMO-MRW and RNFLT, respectively. Sectoral mean BMO-MRW values were also significantly associated with age (P < 0.01, Fig. 6, available at http://aaojournal.org) with the adjusted mean rates varying from −1.79 μm/y (inferonasal) to −1.1 μm/y (temporal). The corresponding sectoral mean RNFLT values were consistently less correlated with age (P < 0.02, for all but the temporal sector where P = 0.15, Fig. 6, available at http://aaojournal.org) with the adjusted rates varying from −0.45 μm/y (inferonasal) to −0.03 (temporal). The spatial pattern of mean age-related loss in BMO-MRW and RNFLT in clock-hour segments is shown in Figure 7 and demonstrates a high degree of similarity, confirmed by the correlation between BMO-MRW and RNFLT sectors ranked according to age-related loss (R^2 = 0.94, P < 0.01). The highest rate of age-related loss occurred in the 6 ‘o’ clock sector in both parameters (−1.75 μm/y for BMO-MRW and −0.42 μm/y for RNFLT), while the lowest rates occurred in the 9 ‘o’ clock sector in both parameters (−0.98 μm/y for BMO-MRW and −0.04 μm/y for RNFLT).

Mean global BMO-MRW and RNFLT were positively correlated (r = 0.35, P < 0.01, Fig. 8), however, sectorally the relationship varied notably (Fig. 9), with the highest correlation in the inferotemporal sector (r = 0.45, P < 0.01) and the weakest in the temporal sector (r = 0.01, P = 0.85). The differences in the strength of the correlations were not due to the range of the measurements, for example, the range of two variables were comparable in the

inferotemporal and superonasal quadrants, yet the correlations were remarkably different (Fig. 9).

The age- and BMO-area adjusted prediction limits for BMO-MRW and RNFLT are shown in Figure 10. The median BMO-MRW was thinnest in the temporal sector and widest in the superonasal, nasal and inferonasal ones, while the median RNFLT was thinnest in the temporal and nasal sectors, and widest in the superotemporal and inferotemporal ones. Variability in RNFLT depended more on location compared to BMO-MRW.

DISCUSSION

Phenotyping the normal ONH and RNFL, and constructing accurate normative databases helps the clinician in diagnosing glaucoma. The current study is important because it characterizes, for the first time, indices based on BMO in a normal population acquired and analyzed with respect to the eye-specific orientation of the fovea relative to the ONH.

We confirmed the notable variation in the position of the fovea compared to the ONH[16] or BMO centre.[15] In the current study, the FoBMO angle ranged by 20° between subjects, verifying that large errors in designating sectors to the neuroretinal rim,[15] and RNFLT in the peripapillary retina and macula occur with current methods. Our findings re-emphasize that the FoBMO axis in individual subjects should be the reference axis for image acquisition and sectorization of all ONH, RNFL and retinal thickness measurements.[9]

There are a limited number of studies with actual longitudinal ONH or RNFLT data in healthy subjects,[17–19] most with relatively small sample sizes and short follow-up periods. A likely limitation of these studies is imprecise estimates of the effects of age. On the other hand, studies such as ours with usually larger sample sizes and age ranges, assume that cross-sectional observations are valid surrogates for average longitudinally derived age-related changes.

Most previous cross-sectional studies[20–27] did not find an age-related decline in disc margin based rim parameters in normal subjects. In contrast, in the current study, BMO-MRW decreased significantly with age, at a rate of around 4.0% per decade of life, suggesting that this index is more in line with the decrease in RGCs with age observed in histomorphological studies.[28–30]. The anatomical and geometrical errors in neuroretinal rim measurements associated with conventional disc margin measurements[5] may at least partially explain the poor relationship between conventional rim area and age. The rate of loss of RNFLT was −0.21 μm/y or around 2.1% per decade of life and is within the range of −0.13 μm/y[31] to −0.33 μm/y[18] reported in previous cross-sectional studies of normal subjects imaged with OCT.[32, 18, 31] The strength of the correlation between global mean BMO-MRW and age was similar to that between global mean RNFLT and age, however, in each sector, the correlation was stronger with BMO-MRW.

It is natural to assume that because both BMO-MRW and RNFLT are measurements made perpendicular to the orientation of RGC axon bundles that these measurements should be highly correlated. Surprisingly, while the correlation between mean global BMO-MRW and RNFLT was statistically significant, it was practically weak with mean global RNFLT

explaining only 12% of the variation in BMO-MRW. Among the six sectors examined, mean RNFLT explained between 0% (temporally) to 20% (inferotemporally) of the variation in BMO-MRW. This large range in the strength of the correlations was not an artifact resulting from the measurement range of the two parameters. Instead, there are at least two possible explanations. First, the papillomacular bundle which makes up the majority of the temporal rim and RNFL contains more slender axons,[30] which pass through smaller pores and denser connective tissue in the lamina cribrosa.[33, 34] The temporal rim may as a consequence contain a different proportion of neural tissue compared to the inferotemporal rim where axons pass through larger pores with relatively less dense connective tissue.[33, 34] The relative proportion of neural tissue in the RNFL in different sectors may also vary. Second, it is assumed that there is a corresponding sector-to-sector projection of the RNFL to the rim whereby the RNFL in a given sector makes up the rim in the same ONH sector. There is an incomplete understanding of the path of axons as they traverse the retina, approach the ONH and exit the eye and it is plausible that the projection is more complex and variable around the ONH[35, 36] resulting in the observed variability in the correlation between sectoral BMO-MRW and RNFLT.

There were notable differences in the mean age-related loss among the clock hour sectors for both BMO-MRW and RNFLT, often varying by orders of magnitude. From the perspective of accurate diagnostics, these findings underscore the importance of adjusting normative limits according to location within the ONH or peripapillary retina. There was high spatial correlation between clock hour sectors ranked according to magnitude of age-related loss suggesting similarity between these two parameters in spite of notably different correlations between them.

While the age- and BMO-adjusted BMO-MRW prediction limits were less dependent on sector than the corresponding RNFLT limits, there was a tendency for higher variability in both parameters at the superior and inferior poles. The superior and inferior blood vessel trunks are at least partially responsible for the higher variability, as computation of BMO-MRW or RNFLT does not account for blood vessels. This inherent limitation in current methods, which could adversely affect detection of glaucomatous damage in locations thought to be affected earliest and most frequently,[37] could be alleviated by future algorithms which subtract the contribution of blood vessels within the rim or RNFL tissue.[38]

Because of the large between-subject variability in FoBMO angle, image acquisition and sectorisation of rim and RNFLT values would be expected to have a lower between-subject variability and therefore narrower prediction limits. In turn, the use of these normative values could lead to more accurate diagnostics. A limitation of the current study is that for minimizing examination time, we did not perform paired image acquisition and sectorisation of parameters with the conventional methods, whereby it is assumed that ONH and RNFL sectors according to the fixed horizontal and vertical axes of the image frame represent the same anatomical locations between subjects. Such a comparison could have allowed us to confirm whether FoBMO axis acquisition yielded narrower prediction intervals. In a recent study, Amini and colleagues[16] concluded that adjusting for the disc-fovea angle did not yield better diagnostic accuracy in glaumcoma. However, because data acquisition was not performed according to the disc-fovea angle and the normative limits were derived by

interpolation, it is likely that the methods used in the current study will yield different results. Further studies to determine whether clinicians will benefit from these proposed methods of data acquisition and analysis are now necessary.

Our data are limited to findings in White subjects. While numerous studies have demonstrated statistically significant differences in conventional rim parameters and RNFLT among subjects of different races,[39–44] there is little evidence that employing race-specific databases to subjects yields higher diagnostic accuracy.[45–48] The most plausible explanation for these findings is that the between-subject variation in the structural parameters within one race far exceeds the average difference between the races. Normative values of BMO based ONH parameters, such as those investigated in this study, have not been studied before. It is likely that these new parameters are also different among races and possible that race-specific normative values may help better phenotype the ONH and yield higher diagnostic accuracy. Further studies are underway to characterize these new parameters in other racial groups.

Supplementary Material

Refer to Web version on PubMed Central for supplementary material.

Acknowledgments

Financial Support: Heidelberg Engineering GmbH, Heidelberg, Germany (BCC, SD, CAG, CYM, AFS, CFB), Grants MOP11357 from the Canadian Institutes of Health Research (BCC), EY021281 (CFB); and Center for Disease Control (CAG)

REFERENCES

1. Strouthidis NG, Yang H, Reynaud JF, et al. Comparison of clinical and spectral domain optical coherence tomography optic disc margin anatomy. Invest Ophthalmol Vis Sci. 2009; 50:4709–4718. [PubMed: 19443718]
2. Reis AS, Sharpe GP, Yang H, et al. Optic disc margin anatomy in patients with glaucoma and normal controls with spectral domain optical coherence tomography. Ophthalmology. 2012; 119:738–747. [PubMed: 22222150]
3. Srinivasan VJ, Adler DC, Chen Y, et al. Ultrahigh-speed optical coherence tomography for three-dimensional and en face imaging of the retina and optic nerve head. Invest Ophthalmol Vis Sci. 2008; 49:5103–5110. [PubMed: 18658089]
4. Strouthidis NG, Grimm J, Williams GA, et al. A comparison of optic nerve head morphology viewed by spectral domain optical coherence tomography and by serial histology. Investigative ophthalmology & visual science. 2010; 51:1464–1474. [PubMed: 19875649]
5. Reis AS, O'Leary N, Yang H, et al. Influence of clinically invisible, but optical coherence tomography detected, optic disc margin anatomy on neuroretinal rim evaluation. Invest Ophthalmol Vis Sci. 2012; 53:1852–1860. [PubMed: 22410561]
6. Povazay B, Hofer B, Hermann B, et al. Minimum distance mapping using three-dimensional optical coherence tomography for glaucoma diagnosis. Journal of biomedical optics. 2007; 12:041204. [PubMed: 17867793]
7. Chen TC. Spectral domain optical coherence tomography in glaucoma: qualitative and quantitative analysis of the optic nerve head and retinal nerve fiber layer (an AOS thesis). Transactions of the American Ophthalmological Society. 2009; 107:254–281. [PubMed: 20126502]

8. Strouthidis NG, Fortune B, Yang H, et al. Longitudinal change detected by spectral domain optical coherence tomography in the optic nerve head and peripapillary retina in experimental glaucoma. Investigative ophthalmology & visual science. 2011; 52:1206–1219. [PubMed: 21217108]
9. Chauhan BC, Burgoyne CF. From clinical examination of the optic disc to clinical assessment of the optic nerve head: a paradigm change. Am J Ophthalmol. 2013; 156:218–27 e2. [PubMed: 23768651]
10. Chauhan BC, O'Leary N, Almobarak FA, et al. Enhanced detection of open-angle glaucoma with an anatomically accurate optical coherence tomography-derived neuroretinal rim parameter. Ophthalmology. 2013; 120:535–543. [PubMed: 23265804]
11. Mizumoto K, Gosho M, Zako M. Correlation between optic nerve head structural parameters and glaucomatous visual field indices. Clin Ophthalmol. 2014; 8:1203–1208. [PubMed: 25028533]
12. Pollet-Villard F, Chiquet C, Romanet JP, et al. Structure-function relationships with spectral-domain optical coherence tomography retinal nerve fiber layer and optic nerve head measurements. Invest Ophthalmol Vis Sci. 2014; 55:2953–2962. [PubMed: 24692125]
13. Gardiner SK, Ren R, Yang H, et al. A method to estimate the amount of neuroretinal rim tissue in glaucoma: comparison with current methods for measuring rim area. Am J Ophthalmol. 2014; 157:540–9 e1–2. [PubMed: 24239775]
14. Danthurebandara VM, Sharpe GP, Hutchison DM, et al. Enhanced structure-function relationship in glaucoma with an anatomically and geometrically accurate neuroretinal rim measurement. Invest Ophthalmol Vis Sci. 2015; 56:98–105. [PubMed: 25503459]
15. He L, Ren R, Yang H, Anatomic vs, et al. acquired image frame discordance in spectral domain optical coherence tomography minimum rim measurements. PLoS One. 2014; 9:e92225. [PubMed: 24643069]
16. Amini N, Nowroozizadeh S, Cirineo N, et al. Influence of the disc-fovea angle on limits of RNFL variability and glaucoma discrimination. Invest Ophthalmol Vis Sci. 2014; 55:7332–7342. [PubMed: 25301880]
17. See JL, Nicolela MT, Chauhan BC. Rates of neuroretinal rim and peripapillary atrophy area change: a comparative study of glaucoma patients and normal controls. Ophthalmology. 2009; 116:840–847. [PubMed: 19410941]
18. Leung CK, Yu M, Weinreb RN, et al. Retinal nerve fiber layer imaging with spectral-domain optical coherence tomography: a prospective analysis of age-related loss. Ophthalmology. 2012; 119:731–737. [PubMed: 22264886]
19. O'Leary N, Artes PH, Hutchison DM, et al. Rates of retinal nerve fibre layer thickness change in glaucoma patients and control subjects. Eye (Lond). 2012; 26:1554–1562. [PubMed: 23079756]
20. Funk J, Dieringer T, Grehn F. Correlation between neuroretinal rim area and age in normal subjects. Graefes Arch Clin Exp Ophthalmol. 1989; 227:544–548. [PubMed: 2625212]
21. Tsai CS, Ritch R, Shin DH, et al. Age-related decline of disc rim area in visually normal subjects. Ophthalmology. 1992; 99:29–35. [PubMed: 1741134]
22. Varma R, Tielsch JM, Quigley HA, et al. Race-, age-, gender-, and refractive error-related differences in the normal optic disc. Arch Ophthalmol. 1994; 112:1068–1076. [PubMed: 8053821]
23. Garway-Heath DF, Wollstein G, Hitchings RA. Aging changes of the optic nerve head in relation to open angle glaucoma. Br J Ophthalmol. 1997; 81:840–845. [PubMed: 9486023]
24. Nakamura H, Maeda T, Suzuki Y, Inoue Y. Scanning laser tomography to evaluate optic discs of normal eyes. Jpn J Ophthalmol. 1999; 43:410–414. [PubMed: 10580664]
25. Ramrattan RS, Wolfs RC, Jonas JB, et al. Determinants of optic disc characteristics in a general population: The Rotterdam Study. Ophthalmology. 1999; 106:1588–1596. [PubMed: 10442908]
26. Xu L, Wang Y, Yang H, et al. Size of the neuroretinal rim and optic cup and their correlations with ocular and general parameters in adult Chinese: the Beijing eye study. Br J Ophthalmol. 2007; 91:1616–1619. [PubMed: 17596333]
27. Bourne RR, Foster PJ, Bunce C, et al. The morphology of the optic nerve head in the Singaporean Chinese population (the Tanjong Pagar study): part 1--Optic nerve head morphology. Br J Ophthalmol. 2008; 92:303–309. [PubMed: 18303151]
28. Balazsi AG, Rootman J, Drance SM, et al. The effect of age on the nerve fiber population of the human optic nerve. Am J Ophthalmol. 1984; 97:760–766. [PubMed: 6731540]

29. Mikelberg FS, Drance SM, Schulzer M, et al. The normal human optic nerve. Axon count and axon diameter distribution. Ophthalmology. 1989; 96:1325–1328. [PubMed: 2780002]
30. Jonas JB, Muller-Bergh JA, Schlotzer-Schrehardt UM, Naumann GO. Histomorphometry of the human optic nerve. Invest Ophthalmol Vis Sci. 1990; 31:736–744. [PubMed: 2335441]
31. Demirkaya N, van Dijk HW, van Schuppen SM, et al. Effect of age on individual retinal layer thickness in normal eyes as measured with spectral-domain optical coherence tomography. Invest Ophthalmol Vis Sci. 2013; 54:4934–4940. [PubMed: 23761080]
32. Bendschneider D, Tornow RP, Horn FK, et al. Retinal nerve fiber layer thickness in normals measured by spectral domain OCT. J Glaucoma. 2010; 19:475–482. [PubMed: 20051888]
33. Quigley HA, Addicks EM. Regional differences in the structure of the lamina cribrosa and their relation to glaucomatous optic nerve damage. Arch Ophthalmol. 1981; 99:137–143. [PubMed: 7458737]
34. Jonas JB, Mardin CY, Schlotzer-Schrehardt U, Naumann GO. Morphometry of the human lamina cribrosa surface. Invest Ophthalmol Vis Sci. 1991; 32:401–405. [PubMed: 1993592]
35. Jansonius NM, Schiefer J, Nevalainen J, et al. A mathematical model for describing the retinal nerve fiber bundle trajectories in the human eye: average course, variability, and influence of refraction, optic disc size and optic disc position. Exp Eye Res. 2012; 105:70–78. [PubMed: 23099334]
36. Lamparter J, Russell RA, Zhu H, et al. The influence of intersubject variability in ocular anatomical variables on the mapping of retinal locations to the retinal nerve fiber layer and optic nerve head. Invest Ophthalmol Vis Sci. 2013; 54:6074–6082. [PubMed: 23882689]
37. Quigley HA, Addicks EM, Green WR, Maumenee AE. Optic nerve damage in human glaucoma II. The site of injury and susceptibility to damage. Arch Ophthalmol. 1981; 99:635–649. [PubMed: 6164357]
38. Patel NB, Wheat JL, Rodriguez A, et al. Agreement between retinal nerve fiber layer measures from Spectralis and Cirrus spectral domain OCT. Optometry and vision science : official publication of the American Academy of Optometry. 2012; 89:E652–E666. [PubMed: 22105330]
39. Tsai CS, Zangwill L, Gonzalez C, et al. Ethnic differences in optic nerve head topography. J Glaucoma. 1995; 4:248–257. [PubMed: 19920682]
40. Girkin CA, McGwin G Jr, Long C, et al. Subjective and objective optic nerve assessment in African Americans and whites. Invest Ophthalmol Vis Sci. 2004; 45:2272–2278. [PubMed: 15223805]
41. Zangwill LM, Weinreb RN, Berry CC, et al. Racial differences in optic disc topography: baseline results from the confocal scanning laser ophthalmoscopy ancillary study to the ocular hypertension treatment study. Arch Ophthalmol. 2004; 122:22–28. [PubMed: 14718290]
42. Girkin CA, Sample PA, Liebmann JM, et al. African Descent Glaucoma Evaluation Study (ADAGES): II. Ancestry differences in optic disc, retinal nerve fiber layer, and macular structure in healthy subjects. Arch Ophthalmol. 2010; 128:541–550. [PubMed: 20457974]
43. Girkin CA, McGwin G Jr, Sinai MJ, et al. Variation in optic nerve and macular structure with age and race with spectral-domain optical coherence tomography. Ophthalmology. 2011; 118:2403–2408. [PubMed: 21907415]
44. Knight OJ, Girkin CA, Budenz DL, et al. Effect of race, age, and axial length on optic nerve head parameters and retinal nerve fiber layer thickness measured by Cirrus HD-OCT. Arch Ophthalmol. 2012; 130:312–318. [PubMed: 22411660]
45. Zelefsky JR, Harizman N, Mora R, et al. Assessment of a race-specific normative HRT-III database to differentiate glaucomatous from normal eyes. J Glaucoma. 2006; 15:548–551. [PubMed: 17106370]
46. De Leon-Ortega JE, Sakata LM, Monheit BE, et al. Comparison of diagnostic accuracy of Heidelberg Retina Tomograph II and Heidelberg Retina Tomograph 3 to discriminate glaucomatous and nonglaucomatous eyes. Am J Ophthalmol. 2007; 144:525–532. [PubMed: 17693382]
47. Rao HL, Babu GJ, Sekhar GC. Comparison of the diagnostic capability of the Heidelberg Retina Tomographs 2 and 3 for glaucoma in the Indian population. Ophthalmology. 2010; 117:275–281. [PubMed: 19969365]

48. Girkin CA, Liebmann J, Fingeret M, et al. The effects of race, optic disc area, age, and disease severity on the diagnostic performance of spectral-domain optical coherence tomography. Invest Ophthalmol Vis Sci. 2011; 52:6148–6153. [PubMed: 21421879]

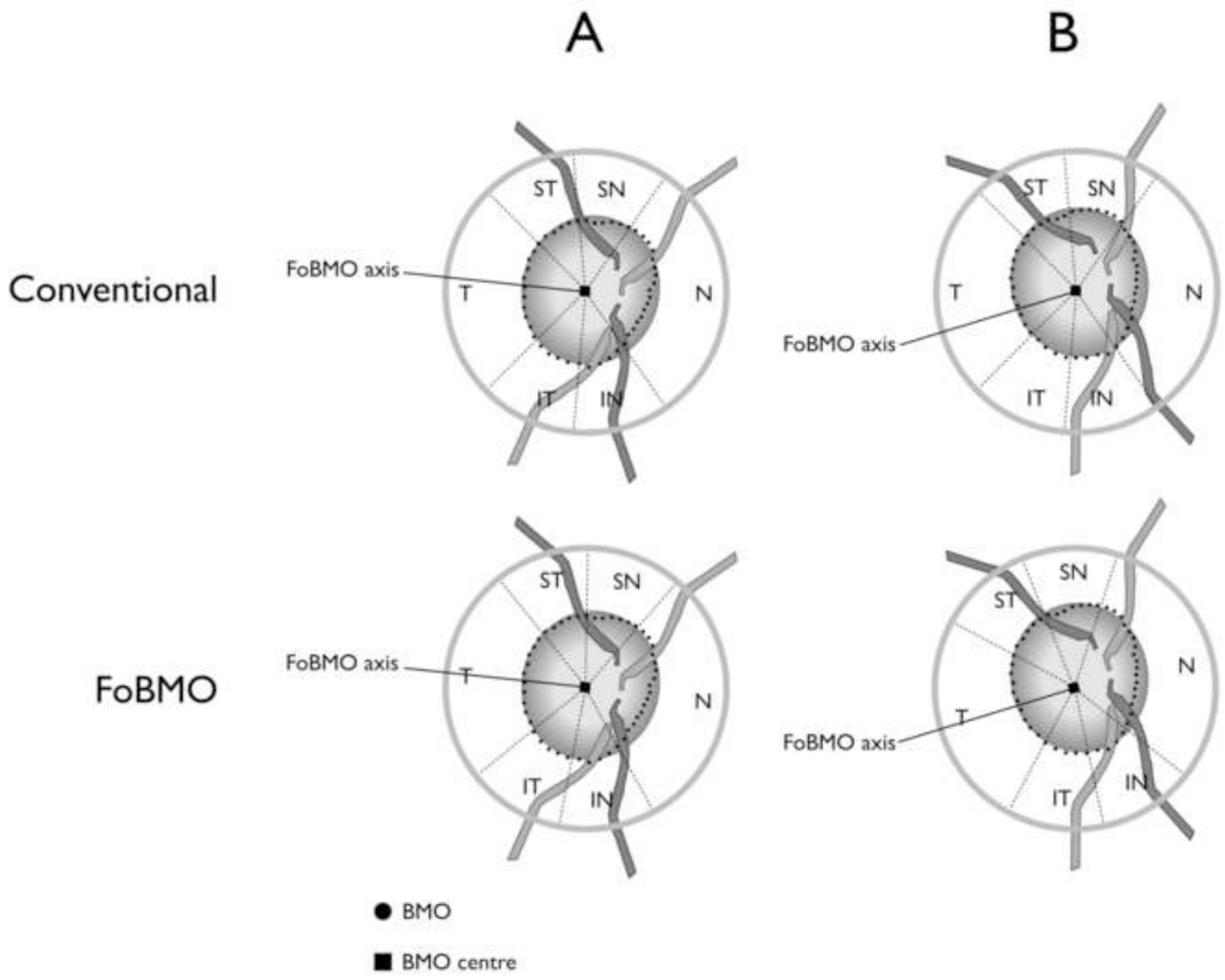

Figure 1.

Schematic illustrating regionalization of neuroretinal rim and peripapillary retinal nerve fiber layer (grey annulus) sectors. With current conventional methods, data acquisition and regionalization relative to the horizontal axis of the imaging frame with the assumption that sectors contain the same anatomical locations. In two cases (A and B) the orientation of the lines connecting the fovea to the Bruch's membrane opening center (FoBMO axis) varies by 20°, hence the sectors contain measurements from different anatomical locations. In FoBMO acquisition and regionalization, sectors contain data from the same anatomical locations. T, temporal; ST, superotemporal; SN, superonasal; N, nasal; IN, inferonasal; IT, inferotemporal

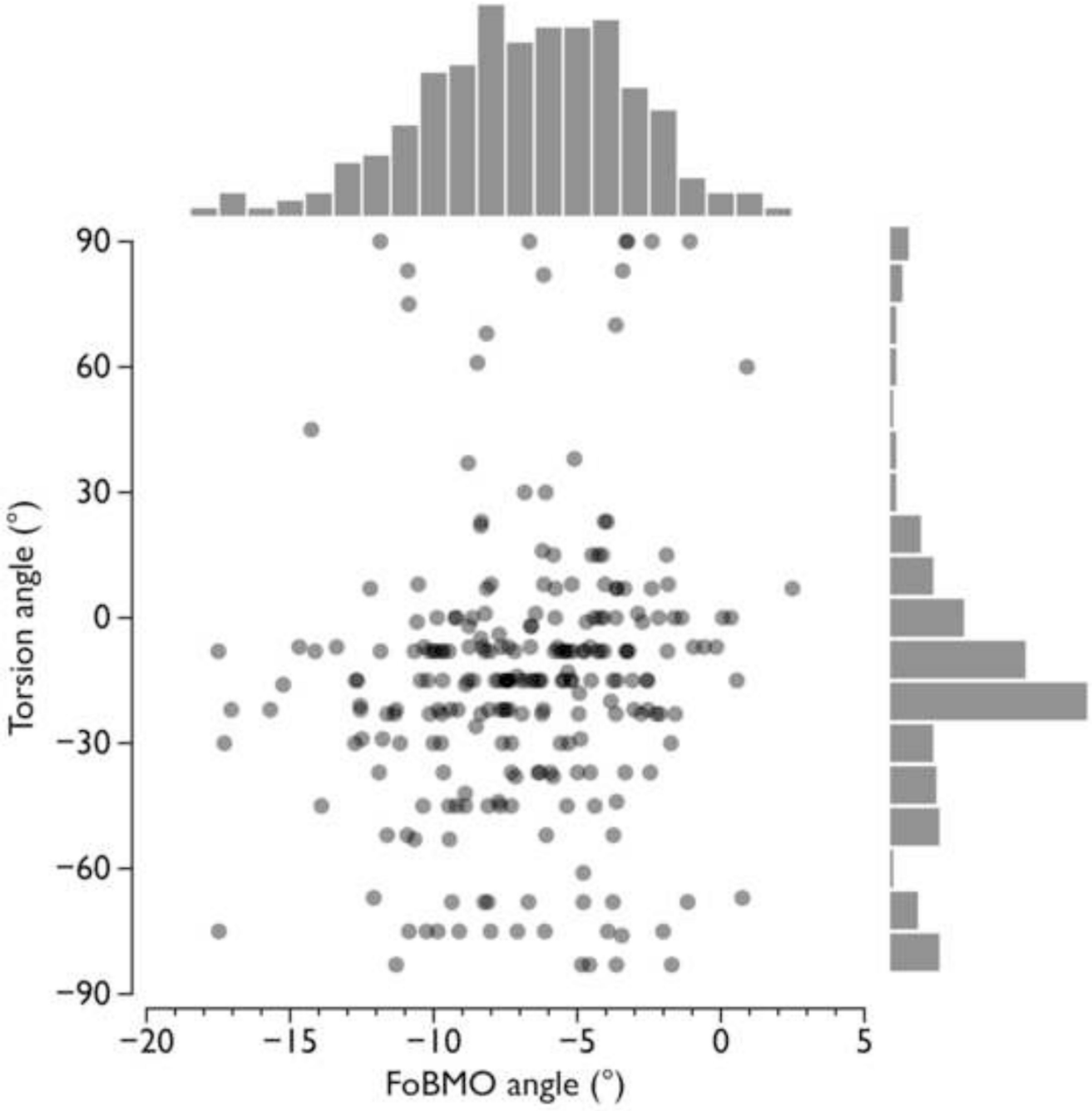

Figure 3.
Relationship between the fovea to Bruch's membrane opening (FoBMO) angle and optic nerve head torsion angle. Histograms for FoBMO angle and torsion angle are also shown.

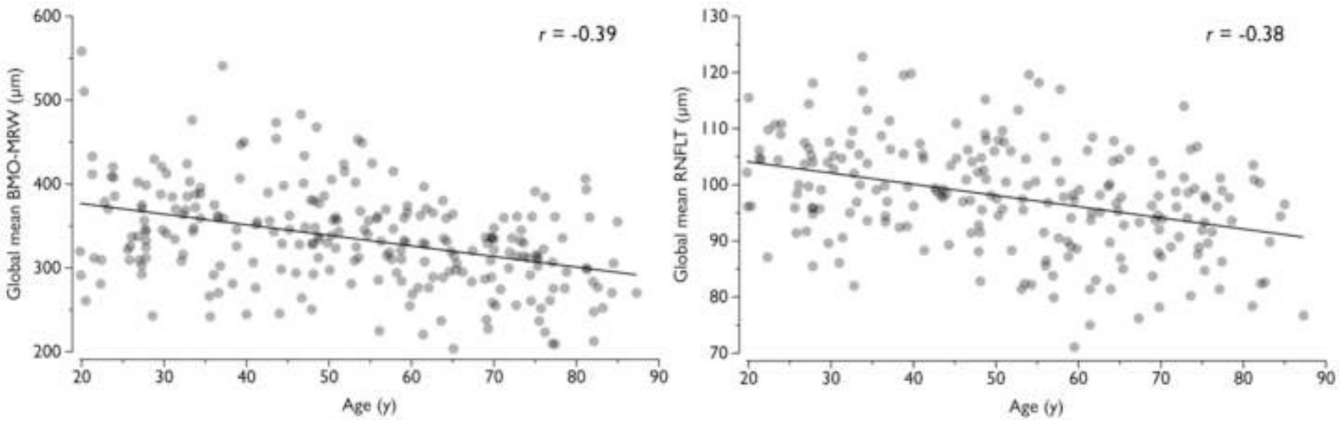

Figure 5.

Age-related loss of global mean Bruch's membrane opening-minimum rim width (BMO-MRW, left) and peripapillary retinal nerve fibre layer thickness (RNFLT, right).

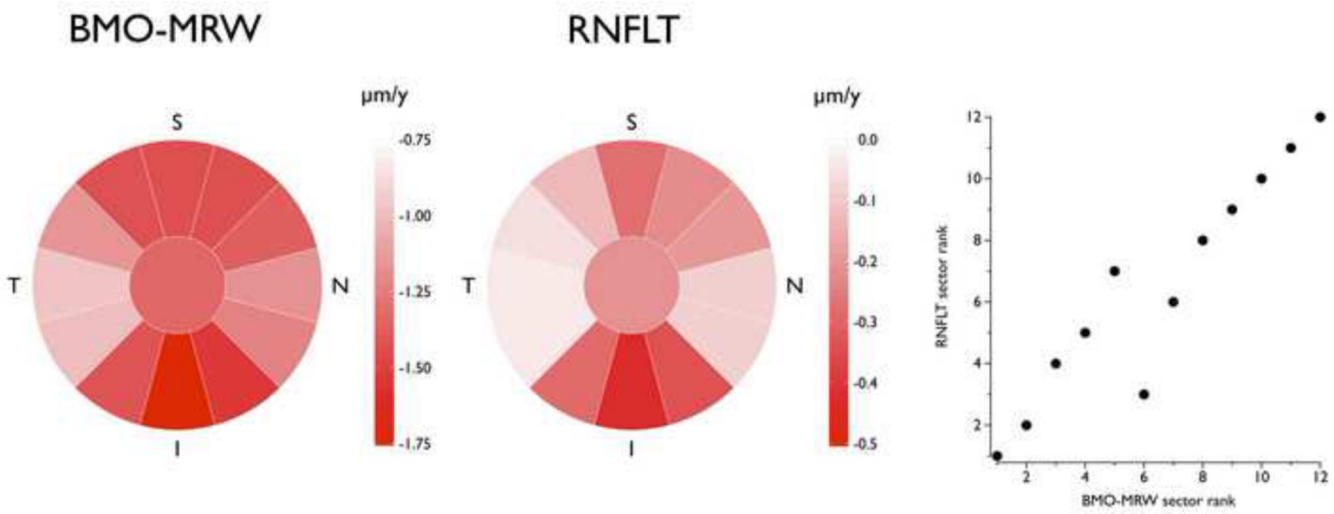

Figure 7.

Age-related loss of mean Bruch's membrane opening-minimum rim width (BMO-MRW, left) and peripapillary retinal nerve fibre layer thickness (RNFLT, centre) in the twelve 30° clock-hour sectors. Mean sector values are colour coded according to the scale in the legend. Rank-order correlation plot (right) showing a high degree of spatial similarity in the rates of BMO-MRW and RNFLT age-related loss.

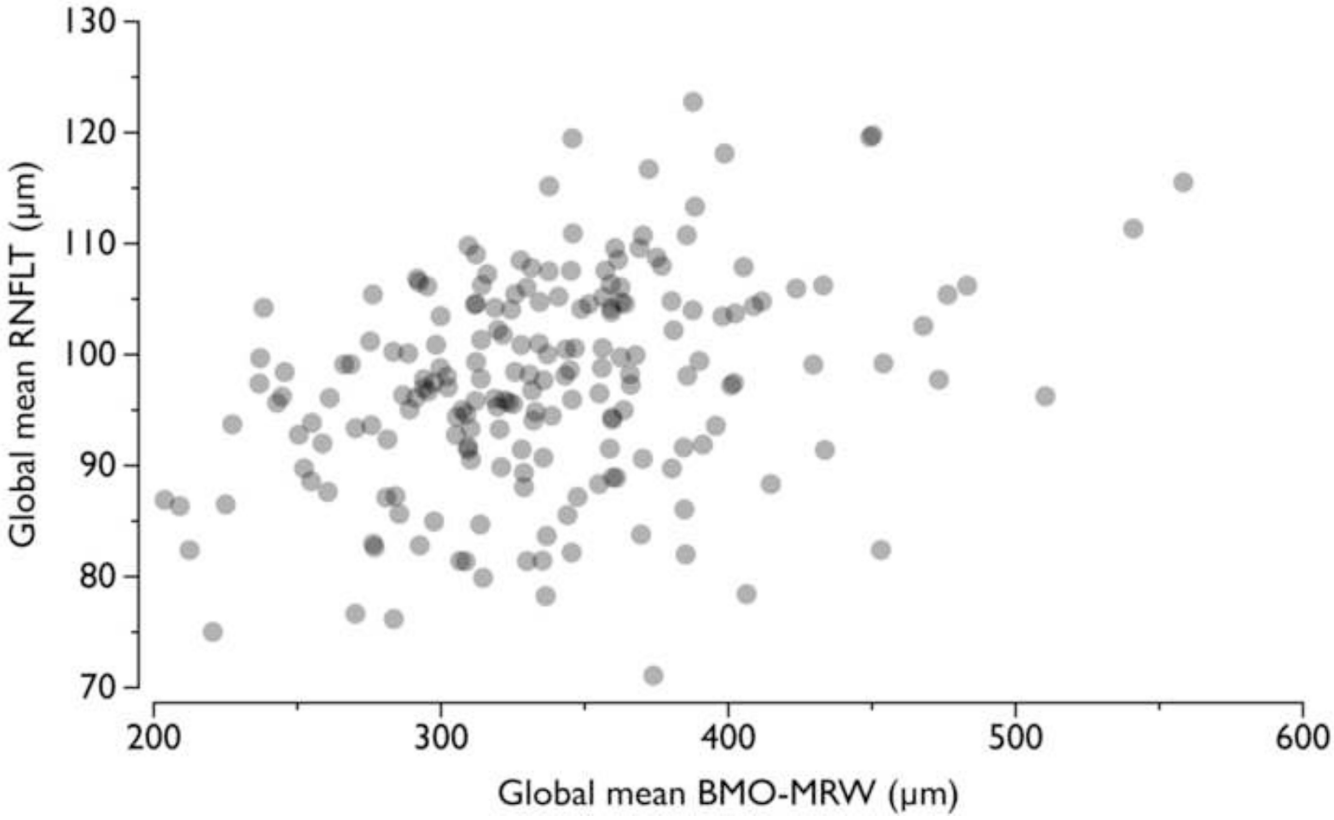

Figure 8.

Correlation between global mean Bruch's membrane opening-minimum rim width (BMO-MRW) and peripapillary retinal nerve fibre layer thickess (RNFLT).

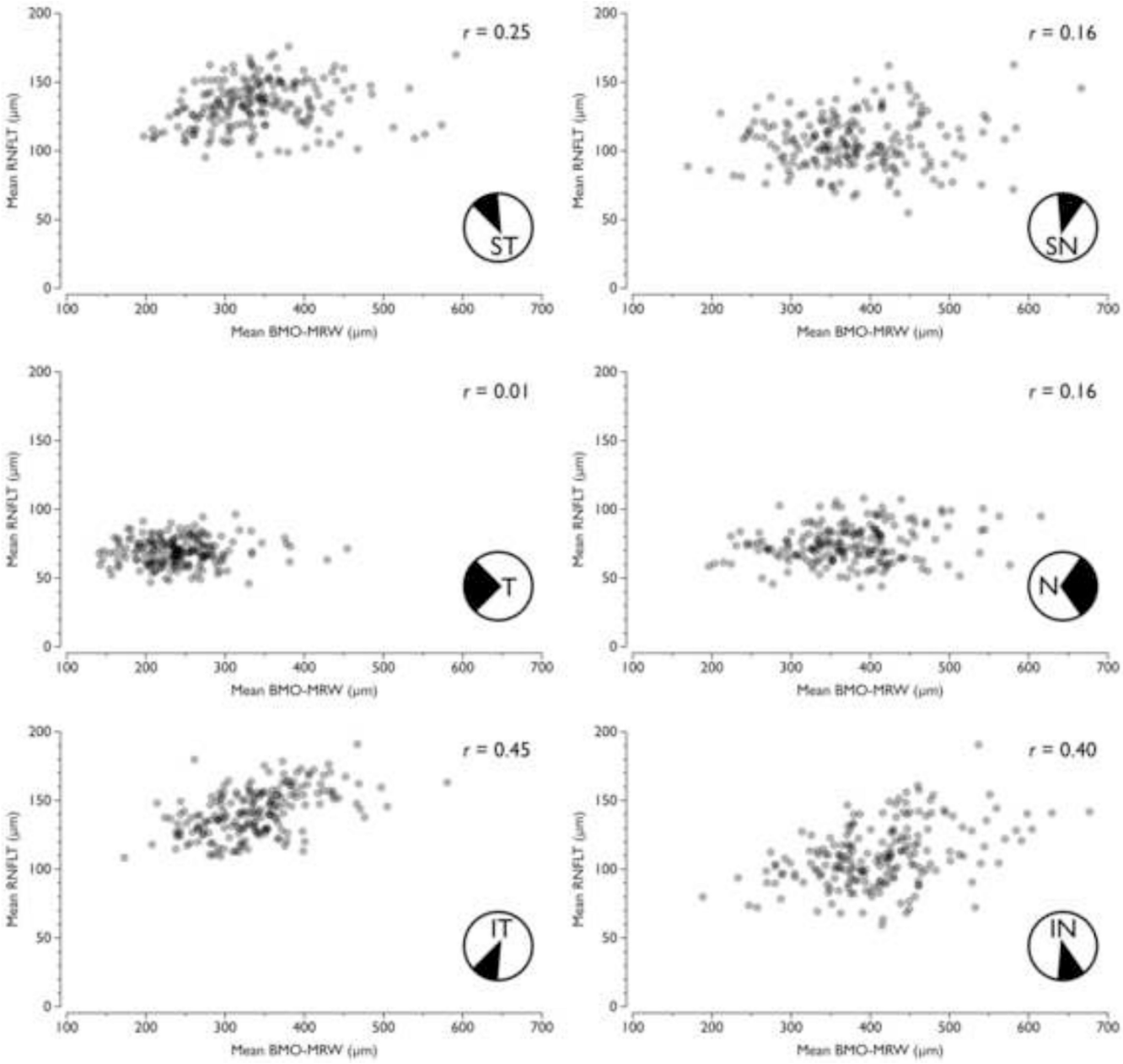

Figure 9.

Correlation between sectoral mean Bruch's membrane opening-minimum rim width (BMO-MRW) and peripapillary retinal nerve fibre layer thickness (RNFLT). T, temporal; ST, superotemporal; SN, superonasal; N, nasal; IN, inferonasal; IT, inferotemporal. Pearson correlation coefficients are shown for each plot.

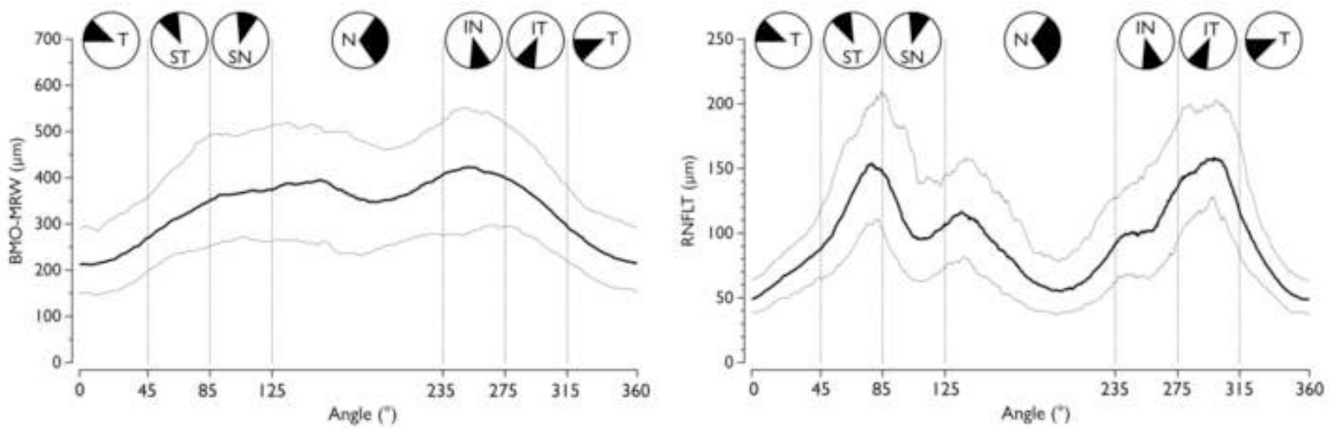

Figure 10.

Covariate adjusted prediction limits for Bruch's membrane opening-minimum rim width (BMO-MRW, left) and peripapillary retinal nerve fibre layer thickness (RNFLT, right). Bold line, 50th percentile; upper faint line, 95th percentile; lower faint line, 5th percentile. T, temporal; ST, superotemporal; SN, superonasal; N, nasal; IN, inferonasal; IT, inferotemporal.